

Fabrication and Characterization of Strained Si Material Using SiGe Virtual Substrate for High Mobility Devices*

Liang Renrong, Zhang Kan, Yang Zongren, Xu Yang, Wang Jing, and Xu Jun†

(Institute of Microelectronics, Tsinghua University, Beijing 100084, China)

Abstract: The fabrication and characterization of strained-Si material grown on a relaxed $\text{Si}_{0.79}\text{Ge}_{0.21}$ /graded $\text{Si}_{1-x}\text{Ge}_x$ /Si virtual substrate, using reduced pressure chemical vapor deposition, are presented. The Ge concentration of the constant composition SiGe layer and the grading rate of the graded SiGe layer are estimated with double-crystal X-ray diffraction and further confirmed by SIMS measurements. The surface root mean square roughness of the strained Si cap layer is 2.36 nm, and the strain is about 0.83% as determined by atomic force microscopy and Raman spectra, respectively. The threading dislocation density is on the order of $4 \times 10^4 \text{ cm}^{-2}$. Furthermore, it is found that the stress in the strained Si cap layer is maintained even after the high thermal budget process. nMOSFET devices are fabricated and measured in strained-Si and unstrained bulk-Si channels. Compared to the co-processed bulk-Si MOSFETs at room temperature, a significant low vertical field mobility enhancement of about 85% is observed in the strained-Si devices.

Key words: strained Si; RPCVD; SiGe virtual substrate; mobility enhancement

EEACC: 2520C; 2560S

CLC number: TN304.1

Document code: A

Article ID: 0253-4177(2007)10-1518-05

1 Introduction

Scaling CMOS under the 65 nm node faces both fundamental limits and technological challenges. One possible way to improve device performance is to enhance carrier mobility using material and process innovations (so-called “mobility engineering”). Strained Si grown on strain relaxed SiGe buffer layers is recognized as a promising way to achieve a global biaxial tensile strained channel. It provides enhanced electron and hole mobilities compared with bulk Si^[1,2]. In order to obtain high quality strained-Si material, it is necessary to fabricate device-quality buffer layers with a very smooth surface and a low threading dislocation density. A number of growth techniques have been developed with demonstrated capability to produce device-quality SiGe films. The reduced pressure chemical vapor deposition (RPCVD) technique is commercially available for large scale production of strained-Si MOSFET technology.

In this paper, the strain state as well as the

surface morphology and threading dislocation density of a strained Si cap layer formed on a relaxed $\text{Si}_{0.79}\text{Ge}_{0.21}$ buffer layer were studied. This buffer layer has a compositionally graded buffer layer that serves as a template. Additionally, the characteristics of the SiGe virtual substrate were also investigated. In order to study the electrical quality of the RP-CVD grown strained-Si films and SiGe virtual substrates, n-MOSFET devices using a 10 nm thick strained-Si/relaxed $\text{Si}_{0.79}\text{Ge}_{0.21}$ virtual substrate and bulk-Si (unstrained) channels were processed and measured.

2 Experiment

The samples were grown on 125 mm Si(001) nominal p-type substrates (resistance in the $2 \sim 7 \Omega \cdot \text{cm}$ range) using an Applied Materials Epitaxial 200 RP-CVD system. The sources of Si and Ge were pure dichlorosilane (SiH_2Cl_2) and germane (GeH_4) diluted at 15% in H_2 , respectively. To further decrease the surface roughness and threading dislocation density, the growth rate and temperature were optimized in the epitaxy process.

* Project supported by the National Natural Science Foundation of China (Nos. 60476017, 60636010)

† Corresponding author. Email: junxu@tsinghua.edu.cn

Received 8 May 2007, revised manuscript received 11 June 2007

10nm strained Si
0.8 μm uniform $\text{Si}_{1-x}\text{Ge}_x$ $x = 0.21$
3 μm graded $\text{Si}_{1-x}\text{Ge}_x$ $x = 0 \sim 0.21$
Si substrate

Fig. 1 Structure of the strained Si material using a SiGe virtual substrate

The growth pressure was fixed to 13.3kPa; the growth temperature was set to 900 and 750°C for the growth of the SiGe and the strained Si cap layer, respectively. Figure 1 shows the structure of strained Si material. Prior to the growth of a 10nm thick strained Si cap layer, a virtual substrate consisting of an approximately 3 μm thick linearly graded $\text{Si}_{1-x}\text{Ge}_x$ (with a nominal final Ge mole fraction of 0.21) layer and of an approximately 0.8 μm thick constant composition $\text{Si}_{0.79}\text{Ge}_{0.21}$ buffer layer was grown.

3 Material properties and characterization

3.1 X-ray diffraction determination of the composition

In order to determine the composition of the SiGe virtual substrate with a non-destructive method, conventional ω - 2θ scans were performed using a Siemens D8 Discover high resolution double crystal X-ray diffractometer. The (004) ω - 2θ scans are plotted in Fig. 2. Under the assumption that the SiGe virtual substrate is fully relaxed, Bragg's law is given by

$$2d_{(004)} \sin\theta = \lambda \quad (1)$$

where λ is the X-ray wavelength and is equal to

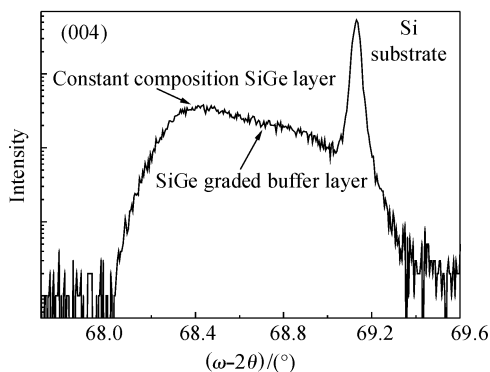


Fig. 2 X-ray double-crystal diffraction ω - 2θ scan curve of the SiGe virtual substrate. The corresponding SIMS profile is plotted in Fig. 3.

0.15406nm in this work, θ is the diffraction angle, and $d_{(004)}$ is the space between crystal planes along the (004) axes.

As for the symmetric (004) reflection, the lattice constant of the diamond alloy structure a_{lat} is given by

$$a_{\text{lat}} = 4d_{(004)} \quad (2)$$

The nonlinear dependence of the SiGe unstrained lattice constant on the Ge mole fraction x can be calculated^[3] by

$$a(\text{Si}_{1-x}\text{Ge}_x) = 5.431 + 0.200326x + 0.02327x^2 (\text{\AA}) \quad (3)$$

For Si (004), the Bragg's diffraction angle θ_0 is equal to 34.5646°. From the X-ray measurement (Fig. 2), the diffraction angle for the constant composition layer is estimated to be 34.2370°. Thus, combining Eqs. (1), (2), and (3), the Ge content can be estimated to be around 22%. The grading rate of the graded SiGe layer is then around 7.33% Ge/ μm , which is consistent with the set-up values in the epitaxy process. The accurate determinations of the Ge composition and the strain relaxation degree require the measurement of both in-plane and perpendicular lattice parameters; details can be found in previous works^[4].

In order to confirm the Ge mole fraction, secondary ion mass spectrometry (SIMS) measurements were carried out on a Cameca SIMS 4500. The measurement results of the Ge concentration depth profile inside the virtual substrate are plotted in Fig. 3. It shows a start at 2%, a grading rate around 7.4% Ge/ μm of the graded SiGe layer, and a constant composition $\text{Si}_{0.79}\text{Ge}_{0.21}$ layer thickness of 0.778 μm . These values further confirm the results obtained by the measurement of DC-XRD.

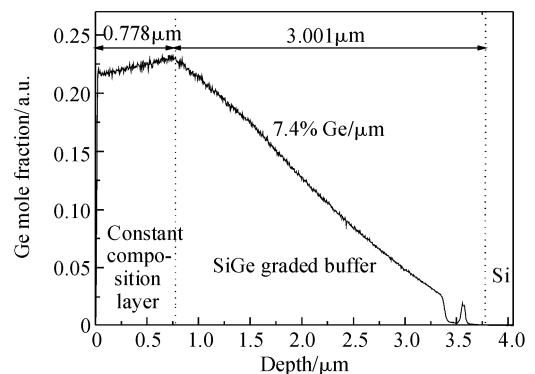


Fig. 3 SIMS depth profile of the Ge mole fraction inside the SiGe virtual substrate layer

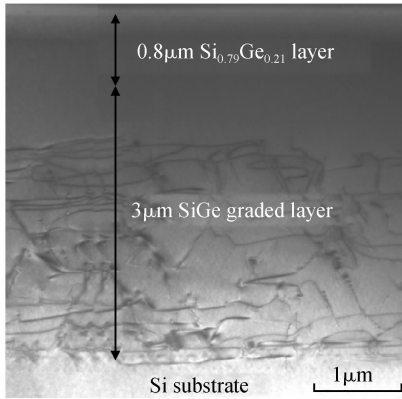


Fig. 4 Cross-sectional TEM image of the SiGe virtual substrate (electron beam along the $\langle 110 \rangle$ axes)

3.2 Dislocation and surface morphologies

The dislocation morphology was analyzed using a JEOL 200CX cross-sectional transmission electron microscope (TEM) operating at 200kV. Figure 4 shows a cross-sectional TEM image of the SiGe virtual substrate. The benefit of using a linearly Ge graded layer is that misfit dislocations spread rapidly towards the edge driven by the residual stress in the films and are thus confined inside the graded layer. It greatly reduces the density of threading dislocations propagating into the strained Si layer^[5,6]. A Schimmel etching solution was used to further depict the dislocations threading penetrating through the constant composition SiGe layer. Counting etch pits with an optical microscope, the statistically obtained threading dislocation density is $4 \times 10^4 \text{ cm}^{-2}$. This result is consistent with the minimum threading dislocation density for relaxed graded SiGe buffer layer with a mismatch of less than 2%, which is in the range of 10^5 to 10^6 cm^{-2} (as estimated by Fitzgerald *et al.*^[7]).

Figure 5 shows an AFM image of the surface morphology of a 10nm strained-Si on $\text{Si}_{0.79}\text{Ge}_{0.21}$ virtual substrate. The root mean square (RMS) surface roughness is measured to be 2.36nm ($10 \mu\text{m} \times 10 \mu\text{m}$). A cross-hatch pattern along the orthogonal $\langle 110 \rangle$ axes is clearly observed.

Figures 6 (a) and (b) display Raman measurements for the 10nm strained Si/ $\text{Si}_{0.79}\text{Ge}_{0.21}$ virtual substrate sample (see Fig. 5) and a reference Si bulk (unstrained) sample for excitation wavelengths of 514 and 325nm, respectively. In Fig. 6 (a), three distinct lines with strain and composi-

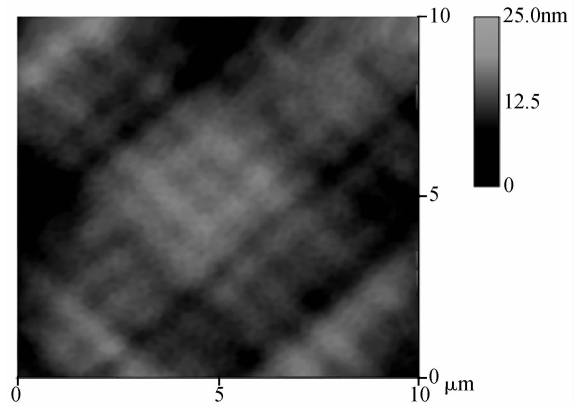


Fig. 5 Tapping-mode atomic force microscopy imaging ($10 \mu\text{m} \times 10 \mu\text{m}$) of the surface of a 10nm strained-Si/relaxed $\text{Si}_{0.79}\text{Ge}_{0.21}$ virtual substrate

tion-dependent energies are found, which are ascribed to^[8] Si-Si vibrations (506.17 cm^{-1}) and localized Si-Si vibrations perturbed by neighboring Ge-Ge (431.93 cm^{-1}) and Si-Ge (404.97 cm^{-1}). The frequency shifts of the Si-Si and Si-Ge lines allow the simultaneous calculation of the composition and residual strain in the SiGe layer using empirical relations for the composition- and strain-induced frequency shift^[9-11]:

$$x_{\text{Ge}} = (37\omega_{\text{Si-Ge}} - 24\omega_{\text{Si-Si}} - 2324.10)/2157.4 \quad (4)$$

$$\epsilon = (68\omega_{\text{Si-Ge}} + 14.2\omega_{\text{Si-Si}} - 34626.52)/2157.4 \quad (5)$$

Solving Eqs. (4) and (5) simultaneously for the data of Fig. 6(a) gives a value of 23.7% for the Ge content and of 0.046 for the residual strain.

Furthermore, various thermal budgets introduced in the MOSFET device fabrication process have an important effect on the strain state in the strained Si cap layer. For example, the activation of the implanted impurity affects the source/drain ohmic contact, and the temperature influences the growth of high quality gate dioxide. In this work, we carefully consider the thermal budget of the growth of high quality gate dioxide. The results are reported in Figs. 6 (b) and 6 (a) (triangles) for excitation wavelengths of 325 and 514nm, respectively. There is almost no shift in the Raman spectra lines of the strained Si cap layer and SiGe virtual substrate before and after oxidation.

Considering that the theoretical value of the strain-shift coefficient of the Si longitudinal optical mode is 830 cm^{-1} ^[12], the observed shift in Fig. 6(b) corresponds to a strain in the Si cap layer of 0.83%. The strain in a 10nm strained Si cap

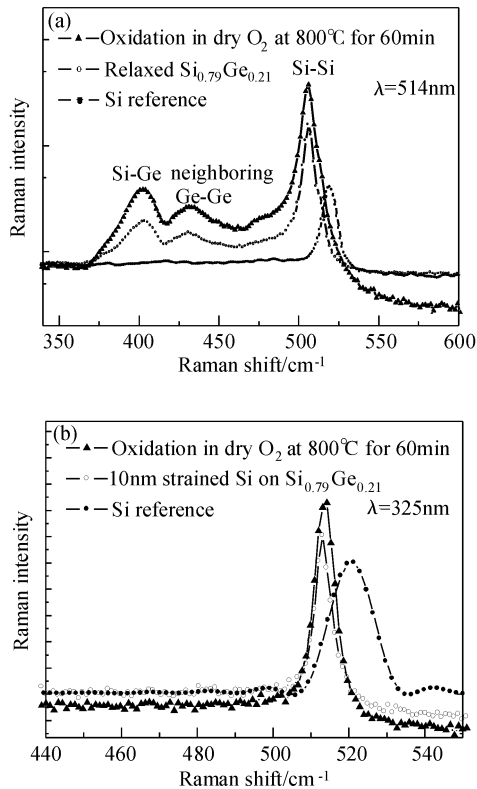


Fig.6 (a) Raman spectra of a 10nm strained-Si/relaxed $\text{Si}_{0.79}\text{Ge}_{0.21}$ virtual substrate for 514nm excitation wavelength; (b) Raman spectra of 10nm strained-Si before/after oxidation for 325nm excitation wavelength

layer formed on fully relaxed $\text{Si}_{0.79}\text{Ge}_{0.21}$ virtual substrate is about 0.82%. All these results confirm that the stress in the strained Si cap layer remains almost the same even after the thermal budget of the device process; this guarantees the improved device performance.

4 Device fabrication and mobility enhancement

To study the electronic quality of strained-Si films, we have fabricated and measured n-MOSFET devices with a 10nm thick strained-Si/relaxed $\text{Si}_{0.79}\text{Ge}_{0.21}$ virtual substrate and bulk-Si (unstrained) channels with a Boron *in-situ* light doping during the epitaxy process. Gate oxides were thermally grown to a thickness of 8.5nm at 800°C. The highest temperature step was the source/drain rapid thermal annealing for 15s at 950°C. The total thermal budgets were carefully controlled to minimize strain relaxation, Ge out-diffusion, and strained-Si consumption during the

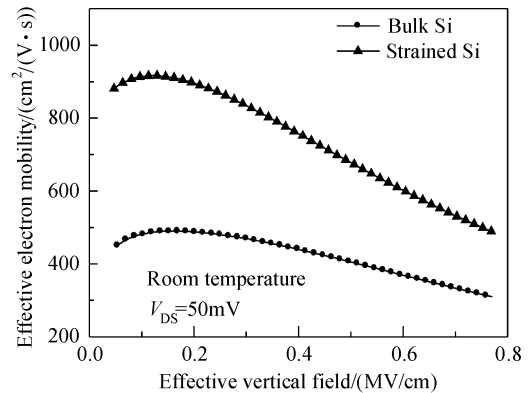


Fig.7 Experimental effective electron mobility versus effective vertical field for strained-Si and bulk Si devices at room temperature

process.

In Fig. 7, the effective electron mobilities for both strained Si and bulk-Si measured in long channel devices are shown as a function of the effective vertical field. The electron mobility of the strained-Si device is enhanced by $\sim 85\%$ at low field and by $\sim 60\%$ at high field compared to the bulk-Si device. This result is consistent with that obtained by Rim *et al.*^[13]. Although there is significant degradation in mobility as the effective vertical field increases for both strained-Si and bulk-Si control devices, the mobility enhancement factor is considered invariable in the whole effective vertical field, as predicted theoretically for the phonon-limited mobility in strained-Si MOS inversion layers^[14]. The strained Si cap layer is thick enough and results in low interface state densities. Coulomb scattering is not the dominant scattering mechanism, and phonon and surface roughness scattering for the strained-Si and control bulk-Si materials make the electron mobility decrease at the same rate with an increasing effective vertical field^[15].

5 Conclusion

We have studied the fabrication and characterization of strained-Si material using SiGe virtual substrate fabricated by RPCVD. The linear grading rate in the graded $\text{Si}_{1-x}\text{Ge}_x$ layer and the Ge mole fraction of the constant composition SiGe film were estimated by DC-XRD, and further confirmed by SIMS. The RMS of the strained silicon surface roughness is 2.36nm, as determined

by AFM measurements; the threading dislocation density is around $4 \times 10^4 \text{ cm}^{-2}$. The strain in the strained Si cap layer is about 0.83% and is unchanged even with the high thermal budget. nMOSFET devices were fabricated and measured on a 10nm thick strained-Si/relaxed $\text{Si}_{0.79}\text{Ge}_{0.21}$ virtual substrate and bulk-Si (unstrained) channels. The low field effective electron mobility of the strained-Si device is enhanced by 85% at room temperature, compared to bulk devices.

References

- [1] Welser J, Hoyt J L, Gibbons J F. NMOS and PMOS transistors fabricated in strained silicon/relaxed silicon-germanium structures. Technical Digest of the International Electron Devices Meeting, 1992; 1000
- [2] Welser J, Hoyt J L, Takagi S, et al. Strain dependence of the performance enhancement in strained-Si n-MOSFETs. Technical Digest of the International Electron Devices Meeting, 1994; 373
- [3] Richard S, Cavassilas N, Aniel F, et al. Strained silicon on SiGe; temperature dependence of carrier effective masses. J Appl Phys, 2003, 94(8): 5088
- [4] Hartmann J M, Gallas B, Zhang J, et al. Gas-source molecular beam epitaxy of SiGe virtual substrates; II. strain relaxation and surface morphology. Semicond Sci Technol, 2000, 15(4): 370
- [5] LeGoues F K, Meyerson B S, Morar J F, et al. Mechanism and conditions for anomalous strain relaxation in graded thin films and superlattices. J Appl Phys, 1992, 71(9): 430
- [6] Fitzgerald E A, Xie Y H, Monroe D, et al. Relaxed $\text{Ge}_x\text{Si}_{1-x}$ structures for III-V integration with Si and high mobility two-dimensional electron gases in Si. J Vac Sci Technol B, 1992, 10(4): 1807
- [7] Fitzgerald E A, Currie M T, Samavedam S B, et al. Dislocations in relaxed SiGe/Si heterostructures. Phys Status Solidi A, 1999, 171(1): 227
- [8] Alonso M I, Winer K. Raman spectra of c- $\text{Si}_{1-x}\text{Ge}_x$ alloys. Phys Rev B, 1989, 39(14): 10056
- [9] Petrova T S, Lyutovich K, Potapova D, et al. Strain and composition in thin SiGe buffer layers with high Ge-content studied by micro-Raman spectroscopy. Proceedings of the Fourth International Conference on Advanced Semiconductor Devices and Microsystems, 2002; 191
- [10] Rath S, Hsieh M L, Etchegoin P, et al. Alloy effects on the Raman spectra of $\text{Si}_{1-x}\text{Ge}_x$ and calibration protocols for alloy compositions based on polarization measurements. Semicond Sci Technol, 2003, 18(6): 566
- [11] Jens S, Gunther V, Frank B, et al. Spectroscopic techniques for characterization of high-mobility strained-Si CMOS. Mater Sci Semicond Processing, 2005, 8(1~3): 267
- [12] Liu R, Canonico M. Applications of UV-Raman spectroscopy and high-resolution X-ray diffraction to microelectronic materials and devices. Microelectron Eng, 2004, 75(3): 243
- [13] Rim K, Hoyt J L, Gibbons J F. Transconductance enhancement in deep submicron strained-Si n-MOSFETs. Technical Digest of the International Electron Devices Meeting, 1998: 707
- [14] Dalapati G, Chattopadhyay S, Kwa K S K, et al. Impact of strained-Si thickness and Ge out-diffusion on gate oxide quality for strained-Si surface channel n-MOSFETs. IEEE Trans Electron Devices, 2006, 53(5): 1142
- [15] Nayfeh H M, Leitz C W, Pitera A J, et al. Influence of high channel doping on the inversion layer electron mobility in strained silicon n-MOSFETs. IEEE Electron Device Lett, 2003, 24(4): 248

采用 SiGe 虚拟衬底高迁移率应变硅材料的制备和表征*

梁仁荣 张 侃 杨宗仁 徐 阳 王 敬 许 军†

(清华大学微电子学研究所, 北京 100084)

摘要: 研究了生长在弛豫 $\text{Si}_{0.79}\text{Ge}_{0.21}$ /梯度 $\text{Si}_{1-x}\text{Ge}_x$ /Si 虚拟衬底上的应变硅材料的制备和表征, 这一结构是由减压外延气相沉积系统制作的. 根据双晶 X 射线衍射计算出固定组分 SiGe 层的 Ge 浓度和梯度组分 SiGe 层的梯度, 并由二次离子质谱仪测量验证. 由原子力显微术和喇曼光谱测试结果得到应变硅帽层的表面粗糙度均方根和应变度分别为 2.36nm 和 0.83%; 穿透位错密度约为 $4 \times 10^4 \text{ cm}^{-2}$. 此外, 发现即使经受了高热开销过程, 应变硅层的应变仍保持不变. 分别在应变硅和无应变的体硅沟道上制作了 nMOSFET 器件, 并对它们进行了测量. 相对于同一流程的体硅 MOSFET, 室温下观测到应变硅器件中电子的低场迁移率显著增强, 约为 85%.

关键词: 应变硅; RPCVD; SiGe 虚拟衬底; 迁移率增强

EEACC: 2520C; 2560S

中图分类号: TN304.1

文献标识码: A

文章编号: 0253-4177(2007)10-1518-05

* 国家自然科学基金资助项目(批准号:60476017,60636010)

† 通信作者. Email: junxu@tsinghua.edu.cn

2007-05-08 收到, 2007-06-11 定稿